Journal of Electroceramics, 15, 167–176, 2005

Electrical Properties of Nb-Doped PZT 65/35 Ceramics: Influence of Nb and Excess PbO

JEAN-CLAUDE M'PEKO[1,2,*], ANTONIO G. PEIXOTO[2], ERNESTO JIMÉNEZ[2] & LUIS M. GAGGERO-SAGER[3]

[1]*Institute of Physics at São Carlos (IFSC), Univ. of São Paulo (USP), P.O. Box: 369, 13560-970 São Carlos – São Paulo, Brazil*
[2]*Department of Physics, Institute of Materials, University of Minho, P-4710057 Braga, Portugal*
[3]*Department of Physics, Faculty of Sciences, Autonomous University of Morelos State, Cuernavaca 62210, Morelos, México*

Submitted March 10, 2003; Revised February 9, 2005

Abstract. The effect of Nb and excess PbO on the structural and electrical properties of conventionally prepared Nb-doped PZT 65/35 ceramics has been studied in this work. It is found that, from excess PbO contents as high as 4 mol%, the solubility limit of Nb in PZT occurs below 4 mol%, while a secondary prevoskite-like phase develops in the dielectric system for a further increase of Nb content. The ferroelectric and piezoelectric properties (permittivity, ferro-paraelectric phase transition, polarization, electromechanical coefficients) of such materials are thus found to be strongly dependent on the degree of densification and structural phase development during sintering at high temperatures. In particular, the nature of the ferro- to para-electric phase transition is in these materials noted to better fit a generalized rather than Smolenskii-Isupov equation, the former being appropriate for the characterization of non-purely diffuse transitions. In nice agreement with the Bokov model, substitution of Nb^{5+} for $(Zr,Ti)^{4+}$ is found to induce only poorly diffuse phase transition in these materials. The electrical properties reported in this work are in magnitude comparable to those exhibited by PZT-based materials.

Keywords: electrical properties, ferroelectric, piezoelectric, PZT-based materials

1. Introduction

Since their discovery, lead zirconate titanate solid solutions, $Pb(Zr_{1-z}Ti_z)O_3$, are widely recognized to represent a special group of perovskite-type $A(B'B'')O_3$ ferroelectric materials with various potential applications in electroceramic and (micro)electronic devices, e.g. as high permittiviy capacitors, piezoelectrics elements, pyroelectric detectors and ferroelectric memories [1–4]. The structure and electrical properties of such solutions, commonly labelled as PZT $100(1-z)/100z$, depend strongly on the Zr/Ti composition ratio. The well-studied diagram phase of the PZT system is characterized by a morphotropic phase boundary (MPB) around $z = 0.47$ corresponding to a transition from a tetagronal to a rhombohedral structure, intermediated by a monoclinic phase (according to recent literature), with decreasing Ti content. The compositions near this MPB region normally show an increased capability of polarization and electromechanical responses, which make them suitable especially for nonvolatile memory and piezoelectric actuator [1–4].

In general, these and other possible applications of PZT-based materials, in bulk as well as in thin film forms, have been and still are explored over a wide range of compositions and (controlled) ion substitution. When doped with La^{3+} substituting for Pb^{2+}, for instance, the PZT solid solution with the 65/35 composition early emerged as a highly promising system due to its high optical transparency and relatively large electrooptic effects, relaxor-type ferro-paraelectric phase transition, etc. [2, 5, 6]. In the case of Nb-doped PZT materials, it has been stated that substitution of a small amount of Nb^{5+} for $(Zr,Ti)^{4+}$ increases considerably the bulk resistivity and reduces aging effects, among

*To whom all correspondence should be addressed. E-mail: jcpeko@yahoo.com/peko@if.sc.usp.br

various effects of relevance [3, 7–10]. Most electrical characterizations of this Nb-doped PZT system have been, however, conducted mainly on thin films and/or over a restricted range of PZT compositions: the MPB region and the range of Zr-rich PZT compositions ($z = 0.03$–0.04), the latter falling within the antiferroelectric region of the diagram phase. The purpose of the present work is the study of the structural and (di)electrical properties of conventionally-prepared Nb-doped PZT ceramics having particularly the Zr/Ti = 65/35 composition out from the conventional MPB.

Reproducibility of stoichiometry of materials has been always a problem of general interest for electroceramics or thin films produced in view of finally performing some physical or chemical activity. For PZT and PZT-based solid solutions, this reproducibility is generally limited by the volatility of lead oxide (PbO) during thermal processing, often allowing to serious variations of final microstructures, phase development, densification and electrical properties of the prepared materials. To prevent lead and oxygen deficiency and, thus, point defects in heat-treated PZT-based samples, some excess PbO is usually added during preparation of PZT-based materials. Depending on the preparation method and conditions, the reproducibility problem is thus often reduced to the finding of the optimal amount of excess PbO to be used, in order to help control the final composition and homogeneity of the produced materials. In the present work, the influence of Nb dopings as well as excess PbO is closely considered. Some previous structural and microstructural results obtained in the laboratory on the system without excess PbO [11] were taken into account for developing this work.

2. Experimental Procedure

2.1. Preparation of the Materials

The materials were prepared by the standard mixed-oxide processing technique, starting from raw powders (TiO_2, ZrO_2, Nb_2O_5 and $PbCO_3$) of high purity grade ($\geq$99.0% in every case). These oxides were mixed in the required amounts so as to give the final composition formula:

$$Pb_{1-x/2}(V_{Pb})_{x/2}(Zr_{0.65}Ti_{0.35})_{1-x}Nb_xO_3 + y\%\ \text{excess PbO}, \quad (1)$$

Table 1. Sintering parameters and final density of the prepared PZTN ceramic samples. ν refers to open porosity.

	Sintering			
PZTN Samples x(Nb%)/y(exc. PbO%)	Temp. (°C)	Time (min.)	ρ_{arch} (g/cm^3)	ν [$= 1 - (\rho_{dim}/\rho_{arch})$]
PZTN 1/0	1200	40	7.73	0.043
PZTN 1/4	1150	40	7.69	0.050
PZTN 1/25	900	30	7.57	0.101
PZTN 4/0	1200	40	7.68	0.086
PZTN 4/4	1150	40	7.41	0.127
PZTN 4/25	900	30	7.22	0.199

abbreviated hereafter as PZTN $100x$/y system, where $x = 0$–0.04 and $y = 0 - 25$. In this formula, incorporation of Nb^{5+} into the perovskite $A(B'B'')O_3$ structure is assumed to occur through substitution for $(Zr,Ti)^{4+}$ ions and through charge-compensation by the creation of Pb^{2+} vacancies (V_{Pb}). Another charge compensation mechanism often considered for Nb^{5+} incorporation into PZT is the donor reaction: $Nb_2O_5 = 2Nb_B + 4O_O^x + 1/2\ O_2\ (gass) + 2e^-$. In practice, the electrons (e^-) normally result trapped at V_{Pb} which act as acceptor defects, decreasing thus the p-type conductivity commonly found in PZT-based materials. In the present work, direct priority is given to the ion vacancy compensation mechanism as the raw materials were purposely mixed in quantities so as to satisfy reaction (1). The mixed powders were calcined at 875°C for 2 h. Then, the so-prepared PZTN powders were compacted into disk-shaped samples under a pressure of $\sim$2.8 ton/cm^2. Typical applied sintering (temperature and time) parameters are presented in Table 1. Values of about 1150–1200°C and 40 min were chosen taking into account previous results obtained in the laboratory [11]. Table 1 also includes the final material density (ρ_{arch}) measured by the Archimedes method, and the estimated values of open porosity (ν) taking into account the density (ρ_{dim}) measured from the material dimensions and weigh. As the excess of PbO increased to $y = 25$, sintering temperature was strongly decreased owing to a trend to obtain rather bodies much more porous at higher heat treatments.

2.2. Characterization of the Materials

The structural phase characteristics of the sintered pellets were analyzed by applying X-ray diffraction (XRD) technique (Philips Diffractometer PW1710 BASED) using CuK_α radiation and a step scan from

$2\theta = 18$ to 80°. For electrical studies, silver (Ag) electrodes were fabricated on both surfaces of the sintered samples by DC-sputtering technique. Measurements of capacitance (C) of the samples were performed in a 7600 Precision LCR Meter over a wide range of temperature (from room to ~450–500°C) and frequency (from 100 to 10^6 Hz). Dielectric permittivity was calculated from C taking into account the sample dimensions. Ferroelectric hysteresis loops were measured in a modified Sawyer–Tower circuit operating at a frequency of 50 Hz. For measuring the piezoelectric activity of the materials, the resonance and anti-resonance method was applied. Poling conditions for this experiment will be specified in the text. The resonance and anti-resonance frequencies were measured using the 7600 Precision LCR Meter. Typical estimated electromechanical parameters were the effective and planar coupling coefficients (k^{eff} and k_{p}). Some approximate values of the Poisson's ratio (σ^{E}) were also calculated. Complementary information for the piezoelectric charge coefficient d_{33} of some samples was measured using a Berlincourt Piezo d_{33}-Meter. Compliance (S_{11}^{E}), piezoelectric strain coefficient (d_{31}) and voltage coefficient (g_{31}) for the most dense materials were also estimated.

3. Results and Discussion

3.1. Structural Characterization

In Table 1 we have shown the behavior of the final samples density and open porosity after the sintering process. On comparing PZTN 1/0 and PZTN 4/0, the results indicate that the increase of Nb in the system leads to a decrease of the final compaction of PZTN. According to previous results obtained in the laboratory, Fig. 1 summarizes some of the most significant features found in the characterization by scanning electron microscopy (SEM) and X-ray diffraction (XRD) of a much complete PZTN $100x/0$ series of samples produced under equal conditions [11]. In good agreement with literature [12], these results indicate that incorporation of Nb in the PZT system allows to an inhibition of grain growth during the material sintering, while revealing, on the other hand, a limit of solubility close to 7 mol% of Nb. The materials' average grain size was determined directly from the SEM micrographs by using the classical linear intercept method [13]. The observed grain growth inhibition most likely result from a grain-boundary pinning process induced by the own

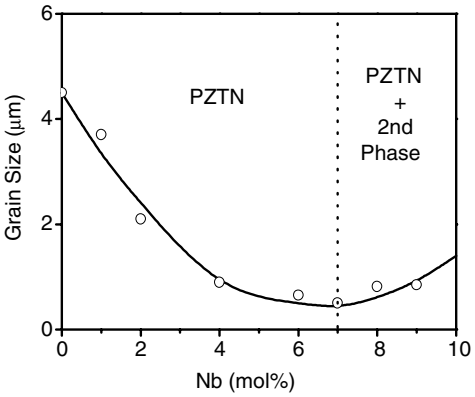

Fig. 1. Average grain size (from SEM), with a measurement error of up to about 28%, and structural phase (from XRD) identified in PZTN ceramic samples with varying Nb content in the system.

presence of (substitutional and/or interstitial) Nb ions at the grain surface. This Nb-induced inhibition process considerably effected the final behavior of density, with the particularity of showing an apparent maximum (of about 7.76 g/cm^3) around $x = 2$ mol% [11]. That is, although strongly coarsed grain materials generally result in porous bodies, too fined grain materials are expected to also show a very similar trend. If a distribution of grain sizes is considered, as often found, the ideal densification of the system should be reached through an optimal mixture of coarsed and fined grains, the fine grains filling the interstices formed by the larger grains. The decreasing behavior of density with increasing Nb from $x/y = 1/0$ to $x/y = 4/0$ in Table 1 is attributed to this material grain size effect. In Fig. 1, the subsequent, apparent increase of the Nb-doped PZT ceramics' average grain size above 7 mol % of Nb should result from the nucleation and a succeeding modest grain growth of the encountered second phase.

As regards the effect of excess PbO (Table 1), the behavior of density and open porosity is slightly different for the two sets of Nb-doped PZT compositions. In the case of PZTN $1/y$, the material density decreases slightly from $y = 0$ to $y = 4$, and strongly to $y = 25$. In the latter case, the estimated fraction of open porosity (v) is approximately twice the relatively few one observed for the sample with 4% of excess PbO. For the PZTN 4/y set of samples, on the other hand, the decrease of the material density is relatively strong for all contents of excess PbO.

In order to better discuss these results, we first of all chose to follow our study with an analysis of the

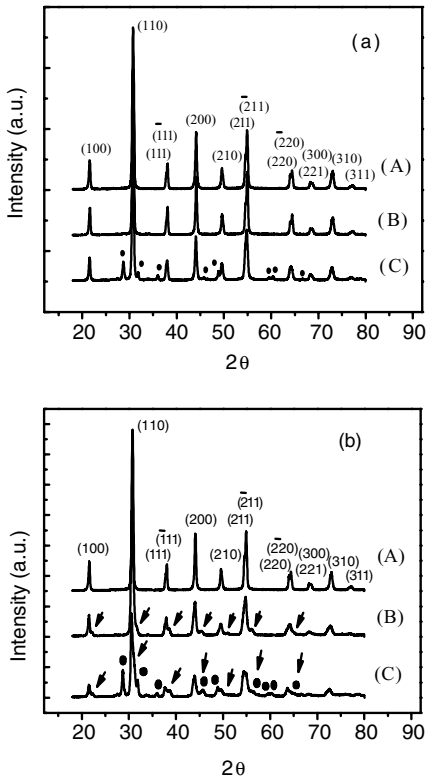

Fig. 2. XRD patterns of the PZTN ceramic samples with compositions (a) $1/y$: (A):PZTN 1/0, (B):PZTN 1/4 and (C):PZTN 1/25; and (b) $4/y$: (A):PZTN 4/0, (B):PZTN 4/4 and (C):PZTN 4/25. Each pattern shows a highly intense perovskite phase isostructural to $Pb(Zr,Ti)O_3$ with Zr/Ti = 65/35. For higher contents of excess PbO ($y = 25$), both compositions (C) are obtained with an additional free PbO phase indicated by closed points. Increasing both Nb and excess PbO ($y = 4$ and 25 in Fig. 2(b)) gives rise to an additional perovskite-like phase (indicated by arrows) coexisting with the main perovskite one.

materials' phase development. Fig. 2 shows the XRD patterns corresponding to the PZTN x/y samples for both $x = 1$ (Fig. 2(a)) and $x = 4$ (Fig. 2(b)). These are characterized by reflection peaks isostructural with the rhombohedral, perovskite PZT 65/35 phase, whose Miller indexes are indicated in the graph. Moreover, it is seen that for the higher content of excess PbO ($y = 25$), the perovskite material has no further tolerance for Pb ions, and a free lead oxide phase (indicated by closed points) develops in the system.

For the PZTN 4/y set of samples (Fig. 2(b)), a close inspection of those spectra corresponding to the compositions with $y = 4$ and 25 revealed the appearance of a second phase (indicated by arrows), besides the principal perovskite structure, and the free lead oxide phase appearing for $y = 25$. From these results it is concluded that, during the PZTN synthesis, high concentrations of both Nb dopant and excess PbO give rise to the formation of a secondary new phase. No attempt was made to characterize in detail this new phase; however, this appears to also be of perovskite type as suggest the positions of its corresponding XRD reflections accompanying regularly those from the principal perovskite phase. The reader should thus note that, while the solubility limit of Nb in PZT 65/35 (i.e. PZTN $100x/0$) corresponded to $x \approx 7$ mol% according to Ref. [11] (Fig. 1), this value is shifted to a lower one ($x < 4$ mol%) when considering the use of an excess PbO content as high as 4% during the material preparation.

To obtain an optimized PZT-based ceramic compactness process, it is well known that a compromise must be in general found between an enhanced excess PbO-induced densification via liquid phase-assisted sintering mechanism *versus* the detrimental effect from its volatilization. In the present work, unfortunately, the latter fact appears to predominate, contributing to lower densities of all PZTN x/y samples with $y \neq 0$ as compared to $y = 0$. When compared to the PZTN $1/y$ set of samples, development of the additional perovskite-like phase in the PZTNs 4/4 and 4/25 ceramics appears to further contribute to a much strong degradation of the whole material density with respect to PZTN 4/0, probably because of altering the optimal grain size distribution for high bodies compaction. We however propose that the lowest densities and relatively high open porosity observed for both PZTN 1/25 (compared to PZTNs 1/0 and 1/4) and PZTN 4/25 (compared to PZTNs 4/0 and 4/4) should mainly arise from void effects associated with a partial evaporation of unreacted excess PbO.

3.2. *Dielectric Properties and Ferroelectric Phase Transition Characterization*

The dielectric permittivity (ε) of all the prepared PZTN samples was studied at various frequencies over a wide range of temperature. The results are illustrated in Figs. 3(a)–(c), and show dielectric peaks characterizing the ferro- to para-electric phase transition. The curves were, in general, weakly frequency dependent, except in the high temperature regime for the highly-porous two samples with $y = 25$ (Fig. 3(c)). This latter picture reflects the typical frequency-dispersion characteristics of materials involving conduction processes and barrier effects induced by the material heterogeneities

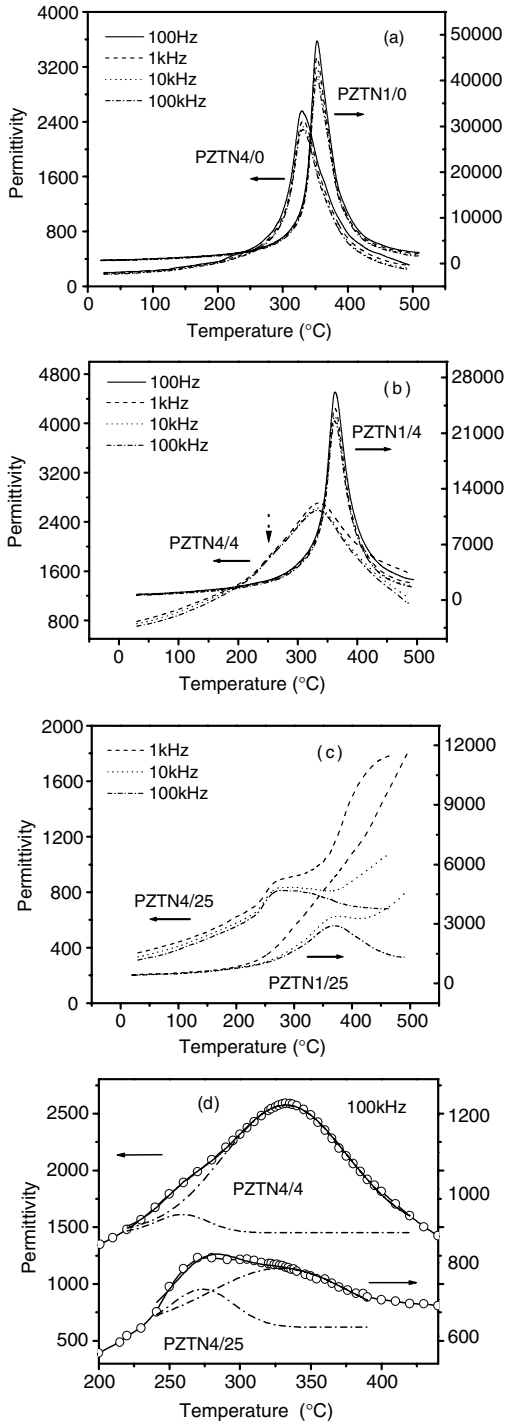

Fig. 3. Temperature dependencies of dielectric permittivity of the studied PZTN $100x/y$ ceramics: (a) $y = 0$, (b) $y = 4$ and (c) $y = 25$. The data correspond to measurements carried out at various frequencies; (d) deconvolution of the PZTN 4/4 and PZTN 4/25 dielectric peaks, for the 100 kHz data, showing two overlapped contributions.

[14–16], i.e. in these samples should develop a considerable amount of space charge whose contribution becomes measurable especially at high temperatures. An additional feature to point out in the cases of $x = 4$ mol% with $y = (4, 25)$, Figs. 3(b) and (c), is the appearance of an additional low temperature dielectric peak (indicated in Fig. 3(b) by an arrow) strongly overlapping the main ferro-paraelectric phase transition. For these two cases, dielectric peak deconvolution is clearly shown in Fig. 3(d). This distinct feature arises from the fact that these PZTN samples contained an additional perovskite-like phase (Fig. 2(b)) to which must correspond this second dielectric peak. This result also suggests that, as well as the principal perovskite phase, the secondary phase is most likely also of ferroelectric type. According to the XRD results presented above, it can be said that this phase formed early during the sintering process, as PZTN 4/25 was sintered at 900°C, and remained stable at higher temperatures, as PZTN 4/4 was sintered at 1150°C.

For the sake of comparison, the processed values of transition temperature (T_m), dielectric permittivity (ε) at 30°C and at T_m (maximum permittivty, ε_m), these latter corresponding to the 1 kHz dielectric data, are summarized in Table 2 for all the samples. On comparing both the PZTN $1/y$ and the PZTN $4/y$ set of samples, it is seen that substitution of Nb^{5+} for $(Zr,Ti)^{4+}$ causes a decrease of the transition temperature (T_m). This result, which remains in good agreement with recent observations, should involve intrinsic perturbations of the ferroelectric micro-domains when the niobium doping is introduced in the perovskite sublattice [17]. An apparent slight shift of this characteristic temperature with increasing excess PbO within the PZTN 1/y set of samples could arise from the activity of excess lead oxide, compensating Pb vacancies in the perovskite structure. The transition temperature of the secondary phase was found to locate at about 265 ± 5°C. The whole behavior of dielectric permittivity closely correlates with that observed for the material density (Table 1) combined with the phase development (Fig. 2). That is, it is seen that the material permittivity decreases in each ceramic system (PZTN $1/y$ or PZTN $4/y$) with increasing excess PbO, as does also the material density. The above results indeed involve the effect of correction to the true material permittivity from contribution of porosity as well as segregation of free PbO phase as in the case of $y = 25$. Such an analysis procedure has been widely considered in the literature [18–22]. Porosity and lead oxide are two phases with lower permittivities

Table 2. Dielectric properties measured for the different PZTN ceramic samples. The parameters γ, C and η characterize deviations from Curie-Weiss law and phase transition features (see text).

Samples	T_m (°C)	ε (30°C)	ε_m	γ	C (10^6°C)	η (°C)
PZTN 1/0	357	746	45283	1.61	6.5	16.3
PZTN 1/4	362	688	24276	1.83	9.1	18.3
PZTN 1/25	365	413	2909	1.90	11.2	55.0
PZTN 4/0	332	192	2418	1.67	1.1	28.7
PZTN 4/4	332	706	2589	1.97	19.5	65.8
PZTN 4/25	330	320	785	–	–	–

than ferroelectric grains. Thus, a decrease of the total permittivity is expected as the volume fraction of these phases increases in the materials.

Regarding the effect of Nb, on the other hand, the smallest value of permittivity found for PZTN 4/0, which however shows a density close to that of PZTN 1/0 (Table 1), should respond to the fact that a Nb-induced decrease of grain size and, thus, increase of the ferroelectric domain density apparently promotes a decrease of domain mobility in these materials [23, 24]. For the PZTN 4/y set of samples, we assume that permittivity initially increased from $y = 0$ to 4 owing to the appearance of the secondary phase (Figs. 2(b) and 3(d)), which we believe is also of ferroelectric nature. A quantitative contribution estimation is here unfortunately unlike because of the lack of detailed information on the real phases connectivity. Nevertheless, considering that softening effects often expected in PZT materials doped with donor-type elements are known to be a source of higher permittivity values (as compared to undoped PZT), it is possible that a second phase-assisted (i) whole-material softening improvement and/or (ii) increment of overall polar orientational possibilities be taken into consideration to totally account for the especially high permittivity value found in PZTN 4/4. If any, however, Nb-induced softening effects from PZTN 1/0 to PZTN 4/0 should result masked apparently owing to the above-mentioned grain size dependent ferroelectric domain mobility effect. The increasing effect of permittivity from $y = 0$ to 4 is seen to be however reduced for $y = 25$, despite the presence of the second phase, as a result of the strong increase of volume fraction of porosity together with segregation of free PbO phase. This phase development should explain why the permittivities from PZTN 1/4 and PZTN 4/4 are basically comparable (within our measuring error: up to about 10%).

Further, the features of the ferro to paraelectric phase transition of the different PZTN samples were closely analyzed. 'Normal' ferroelectric materials are well known to follow the permittivity *versus* temperature dependence described by the Curie-Weiss law:

$$\varepsilon \propto C_W/(T - T_o), \tag{2}$$

where C_W is the Curie Constant and T_o is the Curie-Weiss temperature. From theory, T_o is expected to be less than (first order transition) or equal to (second order transition) the transition temperature. Analysis of our data revealed values of T_o higher than those of T_m. An example of such results, processed for 1 kHz dielectric data, is given in Fig. 4 in terms of the inverse permittivity *versus* temperature behavior for the PZTN 1/0 ceramic sample. The value of the Curie-Weiss temperature resulted in $T_o = 372$°C, while that of the transition is $T_m = 354$°C.

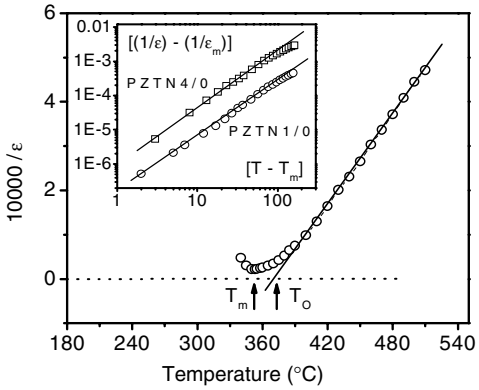

Fig. 4. Curie-Weiss plot for the temperature dependence of permittivity ($1/\varepsilon$ *vs.* T) of the PZTN 1/0 ceramic sample. The inset show log-log plots of $[(1/\varepsilon) - (1/\varepsilon_m)]$ *vs.* $[T - T_m]$ for PZTN 1/0 and PZTN 4/0.

Deviation from the Curie-Weiss law is a typical characteristic of ferroelectric materials exhibiting a Diffuse Phase Transition (DPT), in the sense that their

ε *versus* T spectra involve broad rather than sharp dielectric peaks. In the literature, the appearance of diffuseness has been normally argued in terms of variations in local composition giving rise to distinct microregions, each of which has a slightly different Curie point for its ferro-paraelectric phase transition [21, 22, 25, 26]. A so-called Curie region over which develops a broad rather than sharp dielectric peak must be thus considered. According to Smolenskii and Isupov, the DPT should be described by the quadratic relation [21, 22, 25]:

$$1/\varepsilon = A + B(T - T_m)^2, \tag{3}$$

where $A = 1/\varepsilon_m$ and $B = 1/2\varepsilon_m\delta^2$. The parameter δ, known as the diffuse coefficient, characterizes the diffuseness of the phase transition. Accomplishment of this equation means that treatment of the dielectric data, above the transition temperature, in logarithmic plot of the type $\log(1/\varepsilon - 1/\varepsilon_m)$ *versus* $\log(T - T_m)$ should give rise to linear behaviors whose slope value (γ) are expected to be 2. However, estimated values in this work were different from 2, as shown in Fig. 4 inset for PZTN 1/0 and PZTN 4/0, where the slopes resulted to be $\gamma = 1.61$ and 1.67, respectively. In such cases, the phase transition may be considered as "no purely" diffuse, in contrast to the "pure" DPT described by the Smolenskii-Isupov relation.

The characteristics of DPT in ferroelectric materials have proved, in general, to correspond to variable exponents in the range $1 < \gamma \leq 2$ [22, 25, 26]. From the electrical data interpretation point of view, the characteristics of the phase transition of any ferroelectric material can be argued in terms of a generalized empirical equation of the type:

$$\frac{1}{\varepsilon} - \frac{1}{\varepsilon_m} = \frac{1}{C}(T - T_m)^{\gamma}. \tag{4}$$

When compared to relation (3), it can be proposed from relation (4) that $C = \gamma\varepsilon_m\eta^{\gamma}$, where both γ and η must be regarded as degree of the thermal diffuseness of the phase transition. When the Curie-Weiss law is accomplished ($\gamma = 1$), the experimental value of C would correspond to the Curie-Weiss Constant (C_W) in relation (2), while for $\gamma = 2$ the 'pure' Smolenskii-Isupov DPT dependence, relation (3), is satisfied and $\eta \equiv \delta$. Estimated values of all these parameters from the 1 kHz electrical data are also given in Table 2 for all the samples with $y = 0$ and 4. Because the strong frequency dielectric dispersion observed at high temperatures in the samples with a higher excess PbO ($y = 25$), values of these parameters were in these materials either calculated from the 100 kHz dielectric data or simply discarded.

It is noted that the behavior of the estimated DPT parameters (γ and η) also correlates closely with the material density behavior. Similar results have been also found elsewhere [27]. From a microscopic level, this behavior should be accounted for by the fact of dealing with ferroelectric micro-regions embedded in a non-ferroelectric (porous) medium, allowing to a defect-associated lost of the (i) overall material polar coupling and (ii) apparent local composition homogeneity. We should however point out that, as compared to strong or nearly-strong relaxor diffuse ferroelectric materials [6, 22, 25, 28], these PZTN samples indeed show only a 'partial' rather than a properly or great diffuseness character of phase transition, with relatively poor dielectric peaks broadness (see e.g. Figs. 3(a)–(b)). This is an indication that Nb^{5+} does not here properly or significantly induce DPT. In fact, phase transition in the $Pb(Zr,Ti)O_3$ ferroelectric system, which already has a multiple occupation in the B sites (by Zr and Ti), is of nondiffuse type. The diffuse response of this system becomes significantly induced when the material is doped over the A sites occupied by Pb, as in the case of La-modified PZT [6]. This feature can be accounted for taking into account the model by Bokov [29] on the question of the nature of DPT in relaxor ferroelectric materials. In this model, a great importance is given to the crystallographic site at which the random or near-random distribution of ions is being introduced to induce diffuseness. In the $Pb(Zr,Ti)O_3$ system, Pb is the active ion responsible for ferroelectricity, say ferroactive ion, filling the A sites of the pevoskite structure. According to Bokov model, introduction of disordered ocupancy at these ferroactive sites, as in La-modified PZT [6], should be expected to affect the character of the material phase transition much more significantly than increasing disorder over the non-ferroactive sites [29].

3.3. Ferroelectric Hysteresis Loops Parameters and Piezoelectric Characterizations

To complete a ferroelectric characterization of the PZTN materials, hysteresis loops of the elaborated samples were carried out using a modified

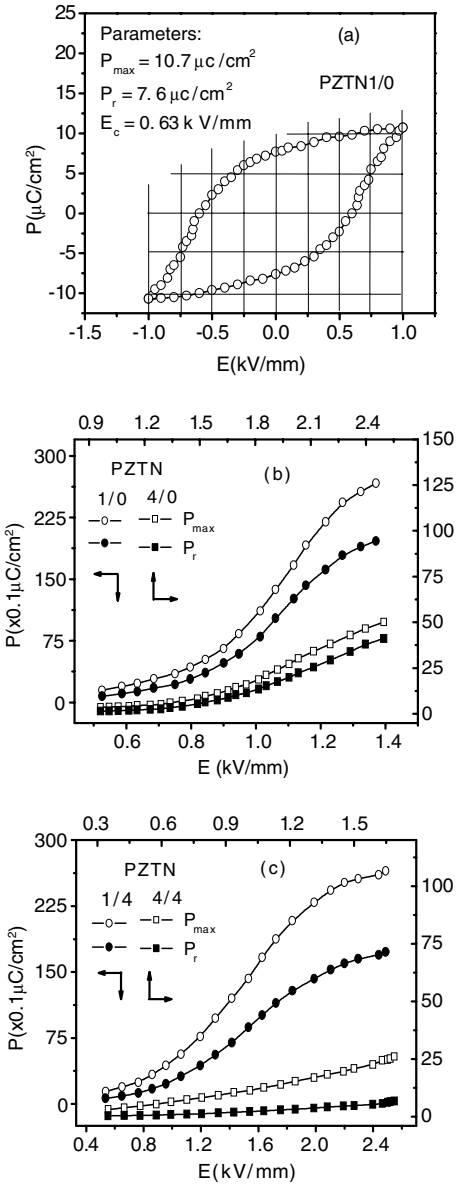

Fig. 5. (a) An example of the ferroelectric hysteresis loop measured for PZTN 1/0. The other figures refer to the electric field dependencies of maximum and remnant polarizations ($P_{\max}$ and P_r) extracted from the ferroelectric hysteresis loops for (b) PZTN 1/0 and PZTN 4/0 and (c) PZTN 1/4 and PZTN 4/4.

Sawyer–Tower circuit. Measurements on the PZTN 100x/y samples with $y = 25$ were practically unlike due to strong conductivity processes, even at relatively low values of applied electric field. Fig. 5(a) shows an example of the ferroelectric hysteresis loop measured for PZTN 1/0, while Figs. 5(b)–(c) summarize the final characteristics obtained for the materials' maximum and remnant polarizations ($P_{\max}$ and P_r) *versus* applied electric field (E). As expected, the curves show increasing behaviors of both properties with increasing the applied field, before showing a saturation process at higher applied electric fields, as can be clearly seen for PZTN 1/0 (Fig. 5(b)) and PZTN 1/4 (Fig. 5(c)), associated to a total or nearly total ferroelectric domain switching. The PZTN 4/4 ceramic sample (Fig. 5(c)) involved relatively high conduction processes, and saturation parameters were not measured to avoid dielectric breakdown, as we observed in some tests.

For comparison, in Table 3 we summarize the different values of the measured hysteresis parameters in these samples, at 1 kV/mm and towards the saturation region. In good agreement with the results obtained from the dielectric permittivity behavior, maximum and remnant polarizations decrease with increasing Nb doping (compare PZTN 1/0 and PZTN 4/0) and excess PbO (compare PZTN 1/0 and PZTN 1/4) in the system. In the case of PZTN 4/4, these parameters increase with respect to PZTN 4/0 due to the fact that this sample contains, as we proposed above from XRD (Fig. 2(b)) and dielectric permittivity (Fig. 3(b)) observations, the contribution of another high-permittivity perovskite phase, besides the main perovskite phase. Notice also in both Figs. 5(b)–(c) that the diminishing behavior of maximum and remnant polaizations mentioned above is accompanied by the fact that the electric field needed to achieve saturation increased with increasing Nb doping and excess PbO. These observations on the effect of Nb on the characteristics of the ferroelectric hysteresis properties ($P_{\max}$ and P_r) of the materials coincide well with those made in the literature in Nb-doped PZT films [8, 9]. In particular, the obtained values of maximum and remnant polarizations for PZTN 1/0 and PZTN 1/4 towards the saturation region (around 26 μC/cm^2) are in the order of, and in some cases slightly higher than, those reported in PZT-based materials [1, 6].

In Fig. 6 are shown the characteristics of coercive field as a function of applied field for some samples. Similarly, this property increases with the applied field before reaching saturation at higher electric fields. This figure also shows that the coercive field saturation process shifts towards higher applied electric fields when increasing Nb and excess PbO. Values of the saturating electric field are given in Table 4 and are found to be lower for the coercive field in comparison to maximum and remnant polarizations. In the region of saturation,

Table 3. Electrical parameters extracted from the ferroelectric hysteresis loops. (E: applied or measuring field; P_{max} and P_r: maximum and remnant polarizations, respectively; E_c: coercive field).

	Values at $E = 1$ kV/mm			Values at saturation		
PZTN samples	P_{max} (μC/cm^2)	P_r (μC/cm^2)	E_c (kV/mm)	P_{max} (μC/cm^2)	P_r (μC/cm^2)	E_c (kV/mm)
PZTN 1/0	10.7	7.6	0.63	26.1	19.6	0.68
PZTN 1/4	4.9	2.7	0.47	25.9	16.8	0.77
PZTN 4/0	0.4	0.15	0.43	3.8	2.8	1.22
PZTN 4/4	1.1	0.22	0.18	–	–	–

Table 4. Values of the saturating electric field for the coercive field (E_c), maximum and remnant polarizations (P_{max} and P_r).

PZTN samples	Saturating electric field (in kV/mm) for E_c	P_{max} and P_r
PZTN 1/0	1.1	1.5
PZTN 1/4	1.6	2.2
PZTN 4/0	1.9	2.5
PZTN 4/4	–	–

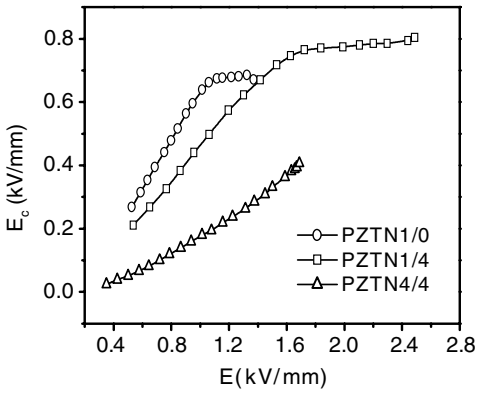

Fig. 6. Electric field dependencies of coercive field (E_c) extracted from ferroelectric hysteresis loops for PZTN 1/0, PZTN 1/4 and PZTN 4/4.

the coercive field rather increases with increasing Nb (compare PZTN 1/0 and PZTN 4/0 in Table 3) and excess PbO (compare PZTN 1/0 and PZTN 1/4 in Table 3).

On the other hand, piezoelectric activity of the materials was measured by applying the resonance and antiresonance method. As presented in Table 5, this experiment was performed in samples poled with an electric field $E_p = 1.09$ kV/mm, at a temperature $T_p \approx 164^\circ$C and for a time $t_p \approx 11$ min. Because of development of high conduction processes, the PZTN 4/4 sample was poled at a lower electric field of 0.75 kV/mm. The electrical data taken from the LCR meter were analyzed in terms of complex impedance and admittance from which the frequencies of maxima and minima were extracted. The piezoelectric constants were finally estimated using conventional procedure reported in the literature [1]. In particular, the estimation of some Poisson's ratio (σ^E) values was achieved by using the method of the frequency ratio of the harmonic resonance to the fundamental resonance, while the coefficient d_{33} was directly measured in a Berlincourt Piezo d_{33}-Meter. For the PZTN 1/0 and PZTN 1/4 samples, which we obtained with the higher electromechanical coefficients, Table 6 shows additional electromechanical coefficients calculated on the basis of the estimated Poisson's ratio values. All the electromechanical coefficients decrease with increasing Nb doping and excess PbO, except S_{11}^E for which the inverse behavior consequently applies. In particular, the value of k_p found for PZTN 1/0 (0.37) is considered to be relatively high, but keeps slightly inferior to those values reached in some piezoelectric PZT compositions, we especially mean at the MPB region [1]. Similarly, the values of d_{33} are in the order of those found in some PZT-based ceramics, but lower than those typically observed, for instance, in "soft" piezoelectric materials ($> \sim$750 pC/N) [1, 4].

4. Conclusions

Both Nb doping and excess PbO have been found to strongly influence phase development and electrical responses of Nb-doped PZT 65/35 ceramics. In particular, Nb shows a clear trend of reducing temperature (T_m) of maximum permittivity (ε_m), while increasing slightly the diffuse nature of the ferro to paraelectric phase transition. However, the PZTN system as a whole is stated to indeed show poor diffuse phase transition

Table 5. Poling conditions and electromechanical coefficients calculated for the PZTN ceramic samples.

Sample	E_p(kV/mm)	T_p(°C)/u_p(min)	k_{eff}	k_p	σ^E	d_{33} (pC/N)
PZTN 1/0	1.09	164/11	0.11	0.37	∼0.34	128
PZTN 1/4	1.09	165/12	0.07	0.27	∼0.32	92
PZTN 4/0	1.09	164/12	0.04	0.21	–	–
PZTN 4/4	0.75	164/11	0.005	∼0.02	–	26

Table 6. Additional electromechanical coefficients calculated for PZTN 1/0 and PZTN 1/4 on the basis of their estimated Poisson's ratios (σ^E). These are the lateral electromechanical coupling factor (k_{31}), the compliance (S_{11}^E) characterizing the elastic behavior at constant electric field, the piezoelectric strain coefficient (d_{31}) and the voltage coefficient (g_{31}).

Sample	k_p	σ^E	k_{31}	S_{11}^E (10^{-11} m^2/N)	d_{31} (10^{-12}C/N)	g_{31} (10^{-3} Vm/N)
PZTN 1/0	0.37	0.34	0.21	2.87	80.81	15.66
PZTN 1/4	0.27	0.32	0.16	3.19	66.10	12.36

characteristics, provided that the introduction of Nb is achieved into the non-ferroactive (Zr,Ti) sites. We also note that the use of high excess PbO contents from 4 mol.% strongly reduces the solubility limit of Nb in PZT. A further increase of Nb beyond this solubility limit induces the appearance of a secondary phase, which notably affects the overall electrical behavior of the PZTN system. In addition, this work shows that the final materials density combined with phase development also influence notably the overall material dielectric properties (permittivities, hysteresis parameters and electromechanical coefficients).

Acknowledgments

The first author (M'Peko) and E. Jimenez acknowledge financial support from FCT, a Portuguese research-funding agency, through Grant No. PRAXIS/CTM/12140/BPD/1/99 and Project PRAXIS XXI/P/CTM/12140/1998.

References

1. B. Jaffe, R.C. William, and H. Jaffe, Piezoelectric Ceramics (Academic Press London and New York, 1971).
2. Y. Yoshikawa and K. Tsuzuki, *J. Am. Ceram. Soc.*, **75**, 2520 (1992).
3. N. Duan, N. Cereceda, B. Noheda, and J.A. Gonzalo, *J. Appl. Phys.*, **82**, 779 (1997).
4. S.-E. Park and T.R. Shrout, *J. Appl. Phys.*, **82**, 1804 (1997).
5. G.H. Haertling, *J. Am. Ceram. Soc.*, **54**, 303 (1971).
6. X. Dai, Z. Xu, and D. Vielhand, *J. Appl. Phys.*, **79**, 1021 (1996).
7. N. Cereceda, B. Noheda and J.A. Gonzalo, *J. Eur. Ceram. Soc.*, **19**, 1201 (1999).
8. R.D. Klissurska, K.G. Brooks, I.M. Reaney, C. Pawlaczyk, M. Kosec, and N. Setter, *J. Am. Ceram. Soc.*, **78**, 1513 (1995).
9. R.D. Klissurska, A.K. Tagantsev, K.G. Brooks, and N. Setter, *J. Am. Ceram. Soc.*, **80**, 336 (1997).
10. C. Tanasoiu, E. Dimitriu, and C. Miclea, *J. Eur. Ceram. Soc.*, **19**, 1187 (1999).
11. A.G. Peixoto, B.Sc. Materials Engineering, University of Minho, Portugal (1998).
12. W. Cao and C.A. Randall, *J. Phys. Chem. Solids*, **57**, 1499 (1996).
13. M.I. Mendelson, *J. Am. Ceram. Soc.*, **52**, 443 (1969).
14. N. Hirose and A.R. West, *J. Am. Ceram. Soc.*, **79**, 1633 (1996).
15. J.-C. M'Peko, J. Portelles, F. Calderón, and G. Rodríguez, *J. Mater. Sci.*, **33**, 1633 (1998).
16. J.-C. M'Peko, *J. Mater. Sci. Lett.*, **19**, 1925 (2000).
17. V. Bornand, D. Granier, P. Papet, and E. Philoppot, *Ann. Chim. Sci. Mat.*, **26**, 135 (2001).
18. Y. Sato, H. Kanai, and Y. Yamashita, *Jpn. J. Appl. Phys.*, **33**, 1380 (1994).
19. M. Arai, J.G.P. Binner, and T.E. Cross, *Jpn. J. Appl. Phys.*, **34**, 6463 (1995).
20. J.-C. M'Peko, Ph.D. Thesis, University of Havana, Cuba (1998).
21. V.A. Isupov, *Ferroelectrics*, **90**, 113 (1989).
22. Y. Park and K.M. Knowles, *J. Appl. Phys.*, **83**, 5702 (1998).
23. W. Cao and C.A. Randall, *J. Phys. Chem. Solids*, **57**, 1499 (1996).
24. D. Remiens, E. Cattan, C. Soyer, and T. Haccart, *Mat. Sci. Semicond. Processing*, **5**, 123 (2003).
25. F.D. Morrison, D.C. Sinclair, and A.R. West, *J. Appl. Phys.*, **86**, 6355 (1999).
26. K. Uchino and S. Nomura, *Ferroelectr. Lett. Sect.*, **44**, 55 (1982).
27. H.R. Rukmini, R.N.P. Choudhray, and D.L. Prabhakara, *Mat. Lett.*, **44**, 96 (2000).
28. D. Viehland, M. Wuttig, and L.E. Cross, *Ferroelectrics*, **120**, 71 (1991).
29. A.A. Bokov, *Ferroelectrics*, **131**, 49 (1992).